SO_2 poisoning mechanism of the multi-active center catalyst for chlorobenzene and NO_x synergistic degradation at dry and humid environment

Guobo Li[a], Kai Shen[a], Peng Wu[a], Yaping Zhang[a*], Yaqin Hu[a], Rui Xiao [a*], Bing Wang[a], Shule Zhang[b]

a. Key Laboratory of Energy Thermal Conversion and Control of Ministry of Education, School of Energy and Environment, Southeast University, Nanjing, 210096, Jiangsu, P. R. China.

b. School of Chemical Engineering, Nanjing University of Science and Technology, Nanjing 210094, P. R. China.

**Corresponding author: Yaping Zhang, Email: amflora@seu.edu.cn, Telephone number: 86-025-8379066 and Rui Xiao, Telephone number: +86-025-83795726, Email: ruixiao@seu.edu.cn*

15

Content

2.1 Catalyst synthesis

The detailed preparation process of $Pd_{0.12}V_4/TiO_2$ is as follows: 4.8 g TiO_2 powder was added to 150 ml of deionized water, and the loading of metal oxide based on atom mass ratios (%) of Pd and V to TiO_2, respectively. 0.0150 g $Pd(NO_3)_2 \cdot nH_2O$, 0.4593 g NH_4VO_3 and 2.0000 g citric acid powder were measured and added. The prepared mixed solution was stirred at 65 °C until a gel, followed by drying at 105 °C for 8 h, and calcined at 500 °C for 5 h in static air. The obtained multi-active center catalyst was called $Pd_{0.12}V_4/TiO_2$ catalyst, simplified as PdV/TiO_2 catalyst. The active component loading rate of the prepared catalyst was tested by inductively coupled plasma mass spectrometry (ICP-MS).

Citric acid, palladium nitrate, ammonium metavanadate, and anatase titanium dioxide (> 99.9 %) were all purchased from Aladdin Reagent Co., Ltd and used as is.

In situ poisoning of the Fresh catalyst was performed using a fixed bed quartz reactor for 24 h at 300 °C. The inlet gas mixture contained (600 ppm) CB, (600 ppm) NH_3, (600 ppm) NO, (600 ppm) SO_2, 10 vol. % O_2 with or without of 10 vol. % H_2O and N_2 as balance. The obtained poisoned catalyst samples could be denoted as Used-H and Used-S, respectively.

Regeneration of poisoned catalysts was performed with the same fixed bed quartz reactor. The catalysts were heated to and kept at 400 °C for 60 min. The inlet gas is only N_2. The obtained corresponding poisoned catalyst samples were denoted as Used-R_H and Used-R_S.

2.2 Catalytic activity measurements

CBCO+SCR activities of the prepared catalysts are conducted in a continuous flow fixed-bed quartz reactor. The inner diameter of reactor is 8 mm and the amount of catalyst used in each experiment is approximately 100 mg (40-60 meshes). The inlet gas mixture contained (600 ppm) CB, (600 ppm) NH_3, (600 ppm) NO, 10 vol. % O_2 with or without of (600 ppm) SO_2 and 10 vol. % H_2O and N_2 as balance, and gas hourly space velocity (GHSV) is 30 000 $ml \cdot g^{-1} \cdot h^{-1}$. The experiments are conducted at an atmospheric pressure of 100-400 °C, and catalysts were stabilized for 30 min at each temperature. The gas concentrations (NO, NO_2, CO, CO_2 and O_2) at the inlet and outlet are detected by flue gas analyzer, while CB and by-products are detected by gas chromatography (GC) equipped with FID. The blank experiment is carried out by using only quartz reactor, and no CB conversion is detected at 400 °C, indicating that CB cannot be oxidized destruction in the selected working condition in absence of a catalyst. The feed gas is mixed to preheat in a chamber before entering the reactor. The Weisz-Prater Criterion was used for testing the effect of internal diffusion, which is as followed:

If $C_{wp}=\frac{-r'_{A(obs)}\rho_c R\rho^2}{DeC_{As}}<1$, then internal mass transfer effects can be neglected.

$-r'_{A(obs)}$= observed reaction rate, kmol/kg -cat·s

R = catalyst particle radius, m

ρ_c = solid catalyst density, kg/m^3; [ρ_c, anatase = 4000 kg/m^3]

D_e = effective gas-phase diffusivity, m^2/s; $=\frac{D_{AB}\varphi_p\sigma_c}{\tau}$

where D_{AB} = gas-phase diffusivity m^2/s; φ_p= pellet porosity; σc=constriction factor; τ =tortuosity. C_{As} = gas concentration of A at the catalyst surface, kmol–A/m^3

$C_{wp}=\frac{-r'_{A(obs)}r_c R^2}{De C_{As}}$=[1×10^{-6} kmol/kg·s]×[4×10^{3} kg/kgm^{3}]×[1.5×10^{-4} kg/kgm^{3}]/[2.6×10^{-4} m^{2}/s] [8.5×10^{-5} kmol/m^{3}]=0.416<1

Thus, the internal mass transfer effects can be neglected.

The CB conversion, NO_x conversion, CO_2 selectivity and N_2 selectivity for the Pd_xV_y/TiO_2 catalysts are calculated according to eq.1-4:

$$CB_{Conversion}=\frac{C(CB)_{in}-C(CB)_{out}}{C(CB)_{in}}\times 100\% \quad (1)$$

$$NO_{x\,Conversion}=\frac{C(NO_x)_{in}-C(NO_x)_{out}}{C(NO_x)_{in}}\times 100\% \quad (2)$$

$$CO_{2\,Selectivity}=\frac{C(CO_2)_{out}-C(CO_2)_{in}}{6\cdot C(CB)_{in}}\times 100\% \quad (3)$$

$$N_{2\,Selectivity}=1-\frac{2C(N_2O)_{out}}{C(NO_x)_{in}+C(NH_3)_{in}-C(NO_x)_{out}-C(NH_3)_{out}}\times 100\% \quad (4)$$

where, $CB_{Conversion}$, $NO_{x\,Conversion}$, $N_{2\,Selectivity}$ and $CO_{2\,Selectivity}$ represent CB conversion, NO_x conversion, N_2 selectivity and CO_2 selectivity, respectively. The $C(CB)_{in}$, $C(CO_2)_{in}$, $C(NH_3)_{in}$ and $C(NO_x)_{in}$ represent the concentration of inlet CB, CO_2, NH_3 and NO_x, respectively. $C(CB)_{out}$, $C(NO_x)_{out}$, $C(NH_3)_{out}$, $C(CO)_{out}$, $C(N_2O)_{out}$, and $C(CO_2)_{out}$ represent the concentration of outlet CB, NO_x, NH_3, CO, N_2O and CO_2, respectively.

Additionally, it is very difficult to establish Cl balance in CBCO reaction. Since the HCl generated in the reaction is preferentially adsorbed on stainless steel pipe at the end of reactor, there is little HCl in the outflow gas, so it is very difficult to quantify.

Assuming that the CBCO reaction in the presence of excess O_2 would follow the first-order reaction mechanism for CB concentration (c): $r = -kc = (-A\exp(-E_a/RT))\cdot c$, where r, k, A, and E_a are reaction rate (mol/s), rate constant (s^{-1}), pre-exponential factor, and apparent activation energy ($kJ\cdot mol^{-1}$), respectively. Arrhenius curves of different

catalysts with CB conversion at <20% at GHSV at 600 000 h^{-1} in the full testing temperature range to ensure a kinetic regime. The detailed information of test results with the influence of internal and external diffusion eliminated is shown in Fig.S1.

The apparent E_a of PdV/TiO_2 catalyst is estimated by the calculation of temperature dependent reaction, and the CB conversion involved in Fig.S1 is lower than 20% to avoid diffusion limitations. As calculated, E_a values of the four obtained catalysts are displayed in Fig.S1, which indicates that the coexistence of Pd and V oxides are beneficial to CBCO and NH_3-SCR.

Turnover frequency (TOF) under different working conditions was calculated according to the transformed mole number of CB (or NO) per second on per mole of Pd center. TOF = CB (or NO) concentration × flow × conversion rate/(22.4 × Pd content × 60), in which CB (or NO) concentration and volumetric flow were 600 ppm and 300 mL/min, respectively, Pd content was calculated according to ICP-MS result.

2.3 Catalyst Characterization

High-resolution transmission electron microscope (HRTEM) images and energy dispersive X-ray spectrometer (EDX) were conducted on Talos F200X microscope operating at an acceleration voltage of 200 kV. X-ray fluorescence (XRF) spectrums were carried out by Bruker S4 Explorer instrument. Powder X-ray diffraction (XRD) patterns were recorded using a Rigaku D/max-2500 diffractometer with Cu Kα radiation source operating at 30 kV. The diffraction patterns were collected over the 2θ range of 10°~80° with a scan speed of $5°\cdot min^{-1}$. The N_2 adsorption-desorption experiments were carried out at liquid N_2 temperature (-196 °C) using a V-Sorb2800P

(Micromeritics ASAP2460, USA) specific surface area and pore size analyzer. The specific surface areas were calculated from N_2 adsorption isotherms by applying the Brunauer-Emmett-Teller (BET) model.[1] Micropore volume and micropore diameter of the catalyst samples were measured by t-plot analyses.[2]

O_2 temperature programmed desorption (O_2-TPD) and H_2 temperature programmed reduction (H_2-TPR) analysis were all conducted in a quartz U-tube reactor connected to an AutoChem1 II 2920 instrument. For TPD measurements, 70 mg of catalyst sample and O_2-He, as adsorbent, were used. The sample was first pretreated in a flow rate of 10 ml/min O_2 and 30 ml/min He at 300 °C. After adsorption saturation, He was purged at 30 ml/min until the TCD detector signal became stable, then, the atmosphere temperature was increased from 100 to 600 °C in a He atmosphere (with a 30 ml/min flow) for desorption, and recording the work curve. Prior to the TPR measurements, a catalyst sample (20 mg) was pretreated at 200 °C for 30 min in high-purity Ar (20 ml/min) and maintain for 35 min, then, cooling down to room temperature. H_2 is introduced at a flow rate of 20 ml/min, subsequently, atmosphere temperature was raised to 800 °C at a rate of 10 °C/min for temperature-programmed reduction, the signal was collected using TCD detector to obtain a H_2-TPR pattern.

X-ray photoelectron spectroscopy (XPS) was performed on a Thermo Scientific K-Alpha$^+$ using Al Kα as the radiation source. The binding energy for Ti *2p*, V *2p*, O *1s*, Pd *3d* and S *2p* was corrected by the surface energy contamination C 1s binding energy peak at 284.8 eV. The actual active metal components were analyzed by ICP-MS with a PerkinElmer NexION 300X spectrometer (USA). Catalyst samples were pre-

dissolved with the help of aqua regia to form a homogeneous solution.

In situ DRIFT (diffuse reflectance infrared Fourier transform) spectra of CB/O_2/NH_3/NO/NO_2 adsorption was conducted on Nicolet6700 spectrometer (Thermo Electron Corporation, USA), with running in the wavenumber ranged 1200-2000 cm^{-1} at a resolution of 4 cm^{-1} (32 scans are taken for each spectrum). The obtained differential catalyst sample spectra were calculated by the Kubelka-Munk function.

2.4. DFT calculations

During all the adsorption calculations, the kinetic energy cutoff was 500 eV. [3] The crystal structure of TiO_2, has tetragonal symmetry with a space group of mp-390. Owing to the large size of slab model (22.23 Å×14.29 Å×20.82 Å), a Gamma-Centered 1×1×1 mesh was adopted for the Brillouin zone integration. The geometry optimization has been performed with the wholead-molecule model relaxing. An at least 20 Å thick vacuum layer in the z-direction is added to simulate surfaces to ensure the reaction will not be influenced by next layer. The convergence criteria for electronic geometry relaxation were set to 10^{-4} eV and 0.01 eV/Å, respectively. Adsorption is only allowed on one side of the exposed surface, with the dipole moment corrected accordingly in the z-direction. The adsorption energy (E_{ads}) of reaction gas on PdV/TiO_2 (101) surface were calculated by using Eq.5:

$$E_{ads}=E_{gas\text{-}structure}-(E_{gas}+E_{structure}) \quad (5)$$

where E_{ads}, $E_{structure}$ and E_{gas} is the total energy of adsorbed reaction gas over PdV/TiO_2 structure (101) surface, interacting PdV/TiO_2 structure (101) surface, and the isolated gas molecules in vacuum, respectively.

The reaction energy (E_r) is defined as Eq.6:

$$E_r = E_{FS} - E_{IS} \quad (6)$$

where E_{IS} and E_{FS} is the energy of initial state and final state, respectively.

Reaction condition information

CBCO: 600 ppm CB + 10 vol.% O_2

SCR: 600 ppm NO + 600 ppm NH_3 + 10 vol.% O_2

CBCO+SCR: 600 ppm CB + 600 ppm NO + 600 ppm NH_3 + 10 vol.% O_2

General properties of the multi-active center catalyst

The general properties of multi-active center catalyst are listed in Fig.S1 and Tab.S1. The structural and morphological properties of it were analyzed by HRTEM (Fig.S1a-b), the lattice spacing was measured to be 0.35, 0.19 and 0.17 nm, which are in good agreement with that of the (101), (200) and (211) crystal plane of the standard TiO_2 (JCPDS PDF# 73-1764). Surface *Brønsted* and *Lewis* acidic sites of the catalyst is probed by Pyridine-IR spectra at 300 °C, which is 29.23 and 202.46 umol/mg respectively, indicating that there are abundant acid sites on the catalyst surface. Pd dispersion on the multi-active center catalyst surface is determined from H_2-O_2 pulsed chemisorption, it is about 0.135%. The detected Pd and V molar ratio of the multi-active center catalyst are 0.112% and 3.606%, respectively, and the results indicating that TiO_2 supported the two active components well. The BET specific surface area of multi-active center catalyst measured at 56.35 $m^2 \cdot g^{-1}$.

Gaseous reaction by-products analysis

Catalytic stability performance of the multi-active center catalyst in different reaction conditions is also test within 24 hours at 300 and 400 °C, respectively. As shown in Fig.S3, the main active centers are more likely to be occupied or overridden by S species at lower temperature (300 °C), especially in humid environment. It is not conducive to the deposition of sulfur species on the catalyst surface at higher temperature (400 °C), while the competitive adsorption between SO_2 (or H_2O) and each reaction gas molecule (CB, O_2, NH_3 and NO_x) still exists on the catalyst surface. This may be the reason for a slightly less in catalytic activity at 400 °C than that condition without SO_2. In addition, 400 °C may be a suitable regeneration temperature for SO_2 poisoning catalysts. The numerical difference between CB conversion and CO_2 selectivity indicated that a part of CB is not completely oxidized to CO_2 during CBCO reaction, which was converted to organic by-products. As shown in Fig.S2, when the reaction equilibrium is achieved at 300 °C, any residual compounds were performed quantitative identify in a calibrated GC-MS system after capturing the reaction exhaust gases, a small amount of polychlorinated by-products (mainly dichloromethane, 1,4-dichlorobenzene, 1,2-dichlorobenzene) and unconverted CB were detected in the three conditions. The generated polychlorinated by-products may be formed from $PdCl_x$ that provided active *Lewis* acidic sites for electrophilic chlorination reaction.[4] Due to the occupation of Pd sites by sulfur species, the adsorption and deep oxidation reaction of transient organic intermediates to CO_2 and H_2O on catalyst surface are hindered. Thus, the organic by-products increase.

Raman analysis

Raman spectroscopy is used to study the oligomerization process of PdO_x and VO_x species on TiO_2 surface and the changes after sulfur and the subsequent thermal regeneration process. Fig.S5 exhibits the Raman spectra of Fresh, Used-S, Used-H, Used-R_S, and Used-R_H catalysts, all spectra are dominated by vibrational fingerprints of anatase-TiO_2 at 396.06, 513.90 and 636.37 cm^{-1}.

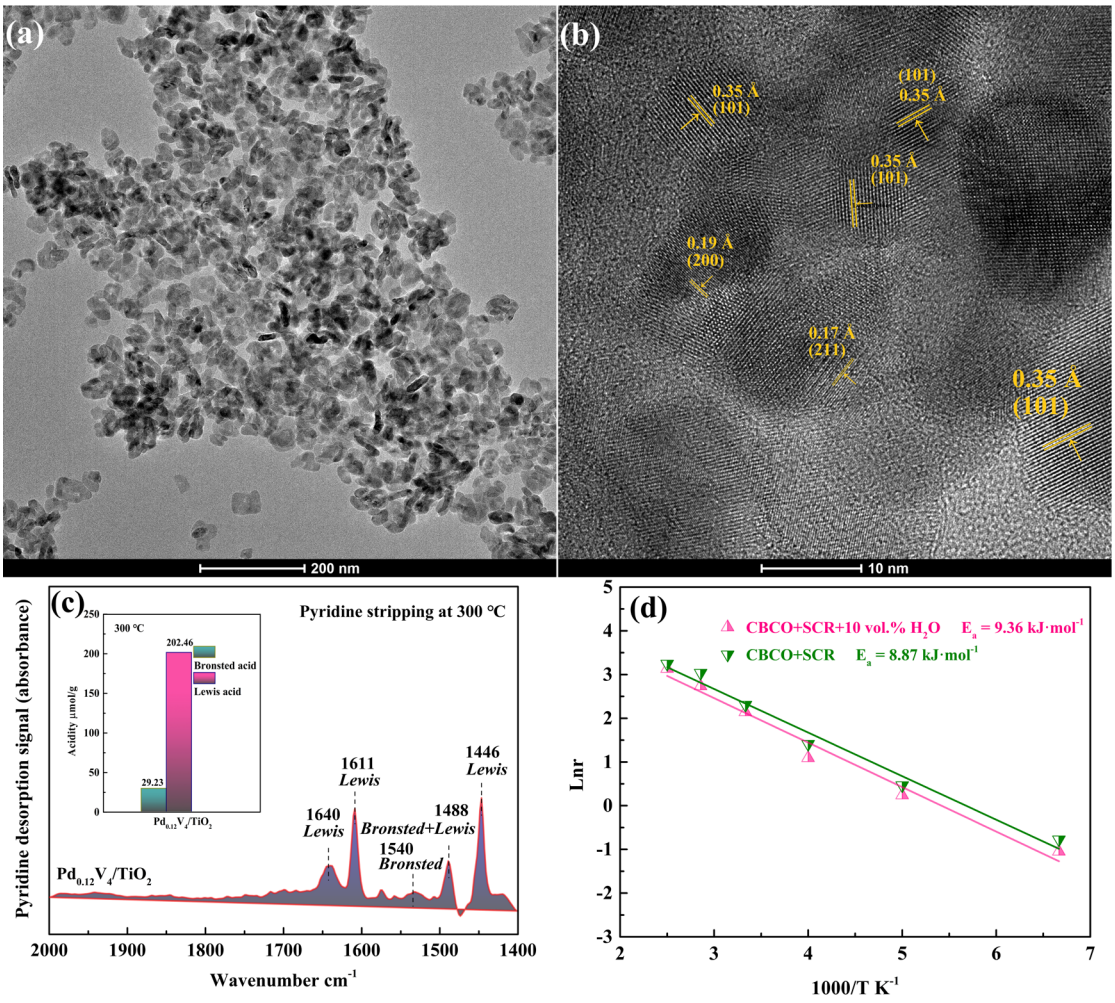

Fig.S1 HRTEM image (a-b) and Pyridine-IR profile (c) analyzed at 300 °C of $Pd_{0.12}V_4/TiO_2$ catalyst.

198 **Tab.S1** Basic information of $Pd_{0.12}V_4/TiO_2$ catalyst.

Catalyst samples	Pd dispersion [a] (%)	Pd molar ratio [b] (%)	V molar ratio [b] (%)	S_{total}[c] (m^2/g)
$Pd_{0.12}V_4/TiO_2$	0.135	0.112	3.606	56.35

199 S_{total}: total BET surface area.

200 a: Determined from H_2-O_2 pulsed chemisorption.

201 b: Determined by ICP-MS and XPS.

202 c: BET specific surface area are determined from the linear part of the BET equation (P/P_0=0.05-

203 0.99).

Tab.S2 The CB turnover frequency (TOF) on $Pd_{0.12}V_4/TiO_2$ catalyst surface with different conditions

Test temperatures (°C)	CBCO+SCR (CB) (mol/s)	CBCO+SCR+600 ppm SO_2 (CB) (mol/s)	CBCO+SCR+600 ppm SO_2+10 vol.% H_2O (CB) (mol/s)
100	0.399×10^{-6}	0.349×10^{-6}	0.309×10^{-6}
150	0.149×10^{-5}	0.798×10^{-6}	0.778×10^{-6}
200	0.319×10^{-5}	0.229×10^{-5}	0.212×10^{-5}
250	0.558×10^{-5}	0.459×10^{-5}	0.435×10^{-5}
300	0.997×10^{-5}	0.878×10^{-5}	0.826×10^{-5}
350	8.75×10^{-5}	4.88×10^{-5}	3.64×10^{-5}
400	9.94×10^{-5}	9.94×10^{-5}	9.90×10^{-5}

Tab.S3 The NO turnover frequency (TOF) on $Pd_{0.12}V_4/TiO_2$ catalyst surface with different conditions

Test temperatures (°C)	CBCO+SCR (NO) (mol/s)	CBCO+SCR+600 ppm SO_2 (NO) (mol/s)	CBCO+SCR+600 ppm SO_2+10 vol.% H_2O (NO) (mol/s)
100	5.68×10^{-6}	2.29×10^{-6}	0.398×10^{-6}
150	1.43×10^{-5}	7.97×10^{-6}	0.698×10^{-6}
200	7.61×10^{-5}	5.58×10^{-5}	0.558×10^{-5}
250	9.96×10^{-5}	8.50×10^{-5}	0.867×10^{-5}
300	9.96×10^{-5}	9.87×10^{-5}	1.83×10^{-5}
350	9.96×10^{-5}	9.90×10^{-5}	3.64×10^{-5}
400	9.46×10^{-5}	8.01×10^{-5}	9.74×10^{-5}

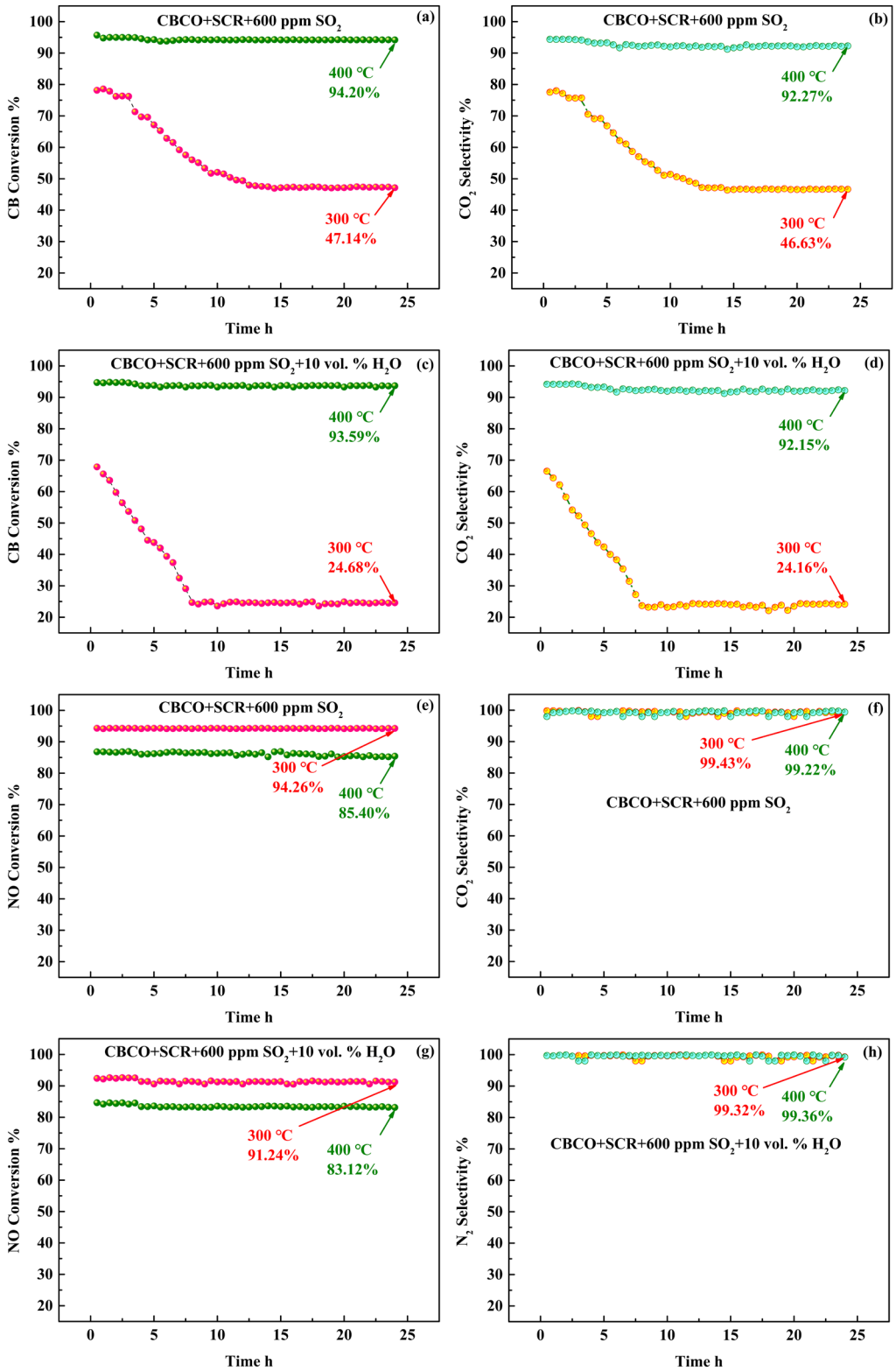

Fig.S2 Effect of 600 ppm SO_2 on CB/NO conversion (a, c, e, g) and CO_2/N_2 selectivity (b, d, f, h) with 24 h in dry and humid (with 10 vol.% H_2O in) environment at 300 and 400 °C, respectively.

Tab.S4 Products in the off Gases from CB oxidation under different stable conditions

No.	Compound name	Molecular formula	Molecular structure
1	Methylene chloride	CH_2Cl_2	
2	Chlorobenzene	C_6H_5Cl	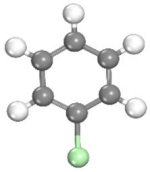
3	1,4-dichlorobenzene	$C_6H_4Cl_2$	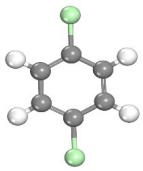
4	1,2-dichlorobenzene	$C_6H_4Cl_2$	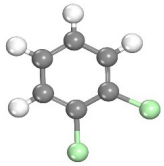

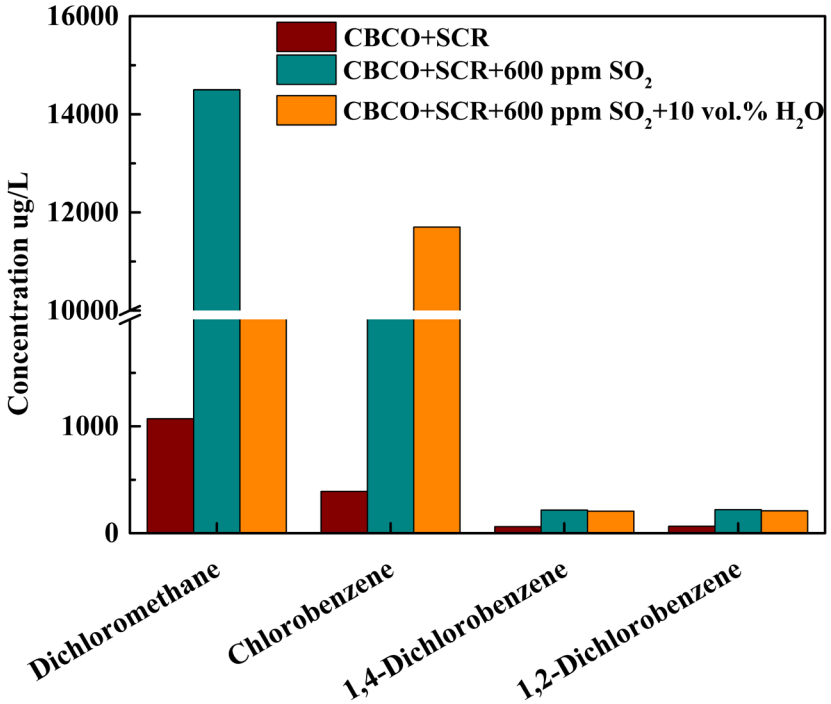

Fig.S3 Gaseous compounds in exhaust gases at 300 °C for $Pd_{0.12}V_4/TiO_2$ catalyst under different conditions.

Tab.S5 Physicochemical properties of different catalysts.

Parameters	Elemental analysis/Atom ratio (%)[a]			Porosity analysis	
	S	V	Pd	S_{total} (m^2/g)[b]	D_{Median} (Å)[c]
Fresh	--[d]	3.34	0.10	56.35	107.49
Used-S	3.39	3.28	0.08	48.15	107.52
Used-H	3.75	3.23	0.07	44.79	107.53
Used-R_S	1.22	3.31	0.09	55.44	107.50
Used-R_H	1.51	3.30	0.09	52.81	107.50

D_{Median}: Median pore diameter

a: Determined by XPS and SEM-EDX.

b: Determined from the linear part of the BET equation (P/P_0=0.05-0.99).

c: Calculated from Horvath-Kawazoe.

d: Not determined.

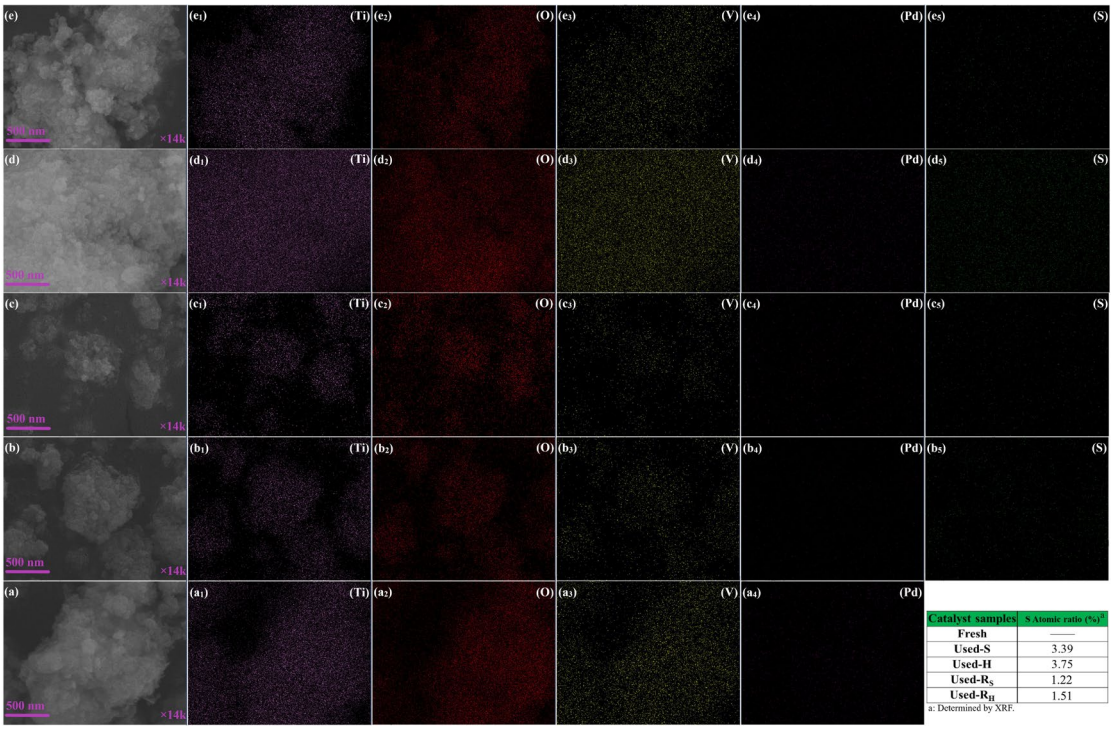

Catalyst samples	S Atomic ratio (%)[a]
Fresh	——
Used-S	3.39
Used-H	3.75
Used-R_S	1.22
Used-R_H	1.51

a: Determined by XRF.

Fig.S4 SEM-EDS mapping images (a-e) of Fresh, Used-S, Used-H, Used-R_S, and Used-R_H catalysts, respectively.

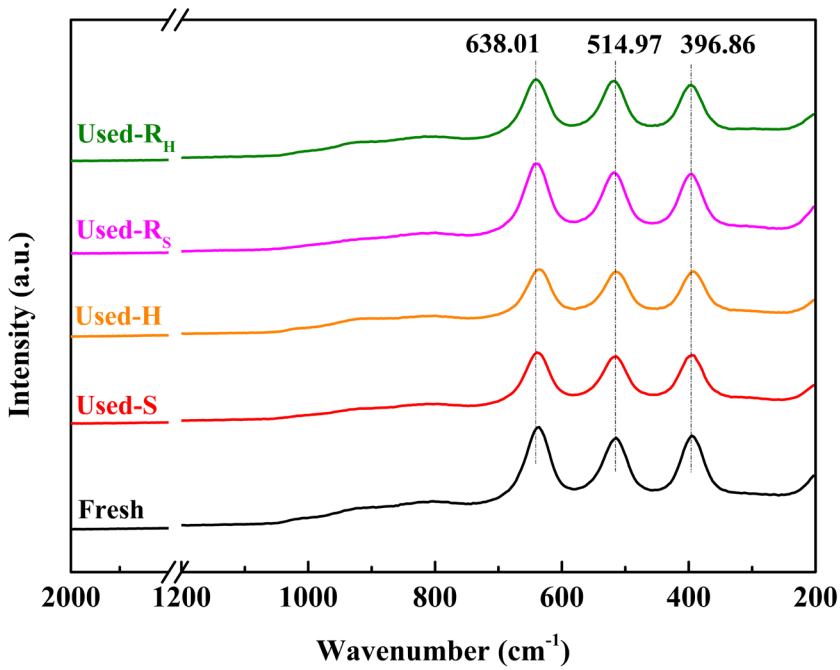

Fig.S5 Raman spectra of Fresh, Used-S, Used-H, Used-R_S, and Used-R_H catalysts, respectively.

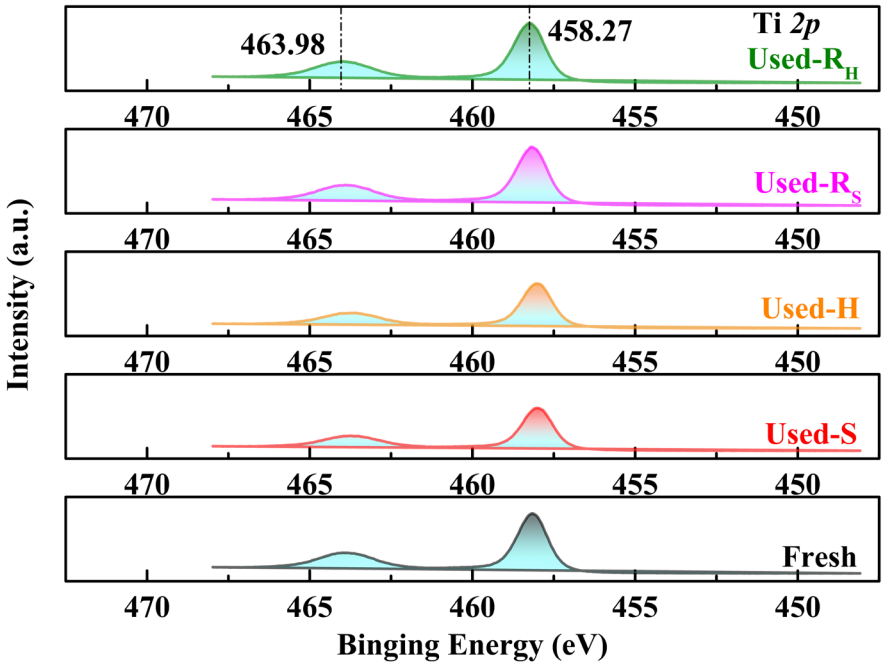

Fig.S6 Ti *2p* XPS profile of Fresh, Used-S, Used-H, Used-R_S and Used-R_H catalysts.

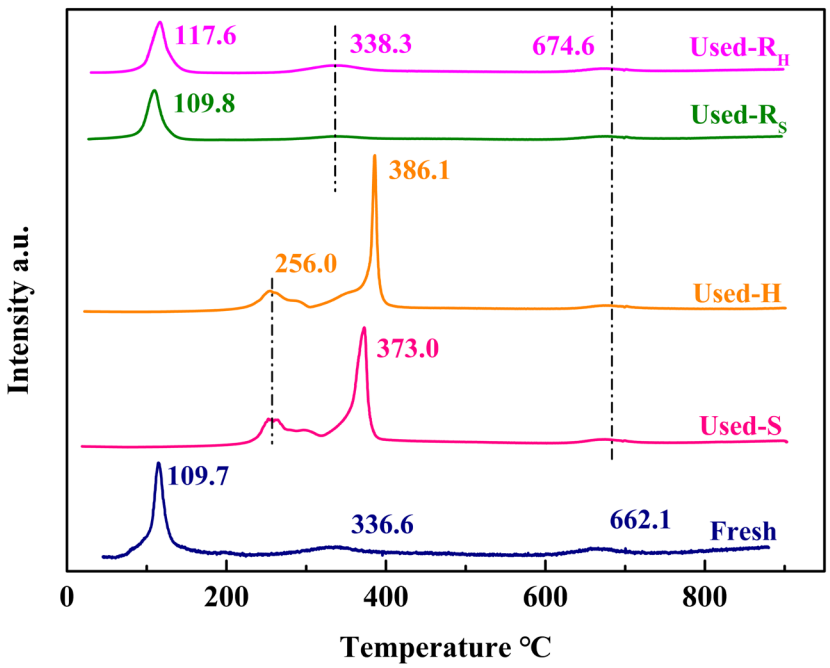

Fig.S7 H_2-TPR profiles of Fresh, Used-S, Used-H, Used-R_S, and Used-R_H catalysts.

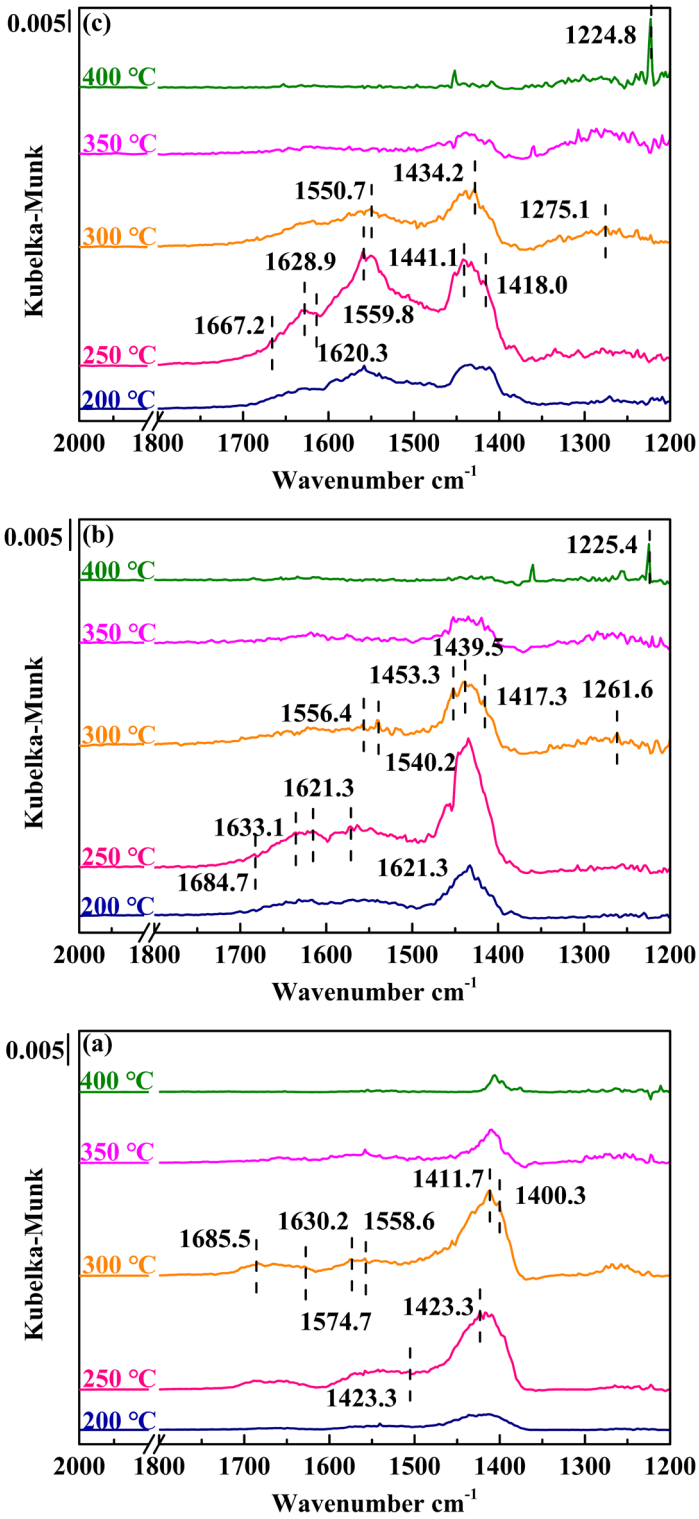

Fig.S8 in situ DRIFT spectra in 1200-2000 cm^{-1} region of different condition (a) CBCO+SCR, (b) CBCO+SCR+ 600 ppm SO_2 and (c) CBCO+SCR+600 ppm SO_2+10 vol.% H_2O on $Pd_{0.12}V_4/TiO_2$ from 200 to 400 °C after the treatment in N_2 at 400 °C. (balanced by N_2), respectively.

Tab.S6 in situ DRIFT spectra peaks and their corresponding species

Wavenumbers (cm^{-1})	Species	References
1224.8, 1225.4	Stretching motion of adsorbed sulfate	4
1261.6, 1275.1	Bidentate sulfates	5
1400.3	Asymmetric stretching vibration of carboxylates with the acetate type	6
1411.7, 1417.3, 1418.0	NH_4NO_3 species	7
1423.3, 1434.2, 1439.5, 1441.1, 1453.3	-N-N-O species	8
1507.6	Maleates	9
1540.2, 1550.7, 1556.4, 1558.6, 1559.8	$-NH_2$	10
1571.2, 1574.7	Gas-phase CB	11
1620.3, 1621.3, 1630.2	Bridging nitrates	12
1628.9	δ(HOH) of adsorbed H_2O	13
1630.2, 1633.1	Chlorinated pbenzoquinone-type	14
1667.2, 1684.7, 1685.5	NH_4^+ species	15

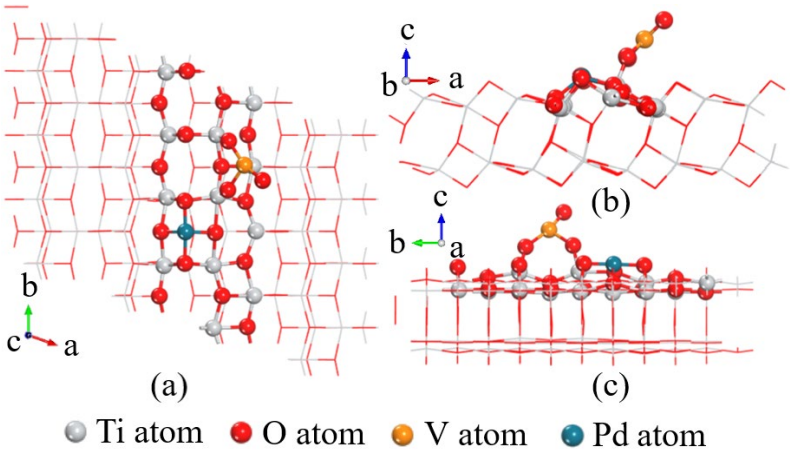

Fig.S9 Top view (a) and side view (b and c) of optimized multi-active center catalyst structure.

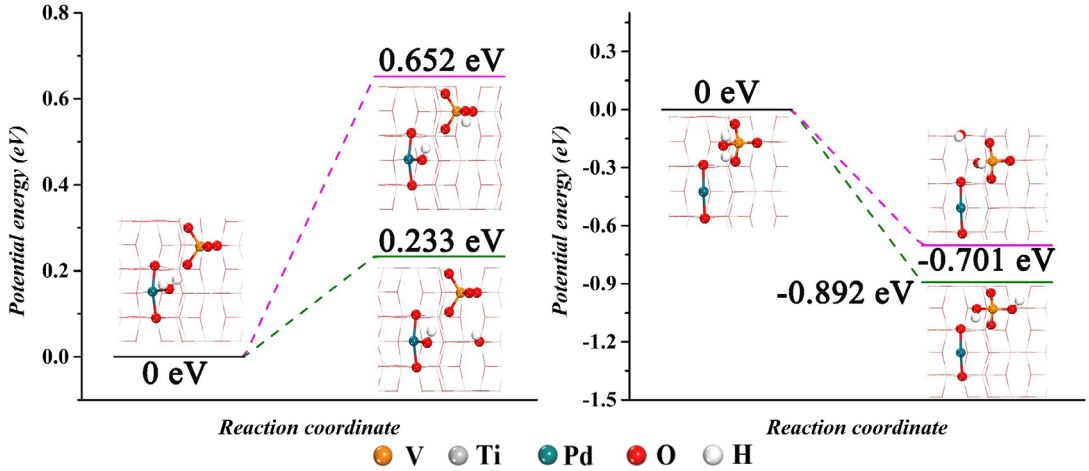

Fig.S10 Dehydrogenation path for single adsorption of H_2O on the multi-active center catalyst surface.

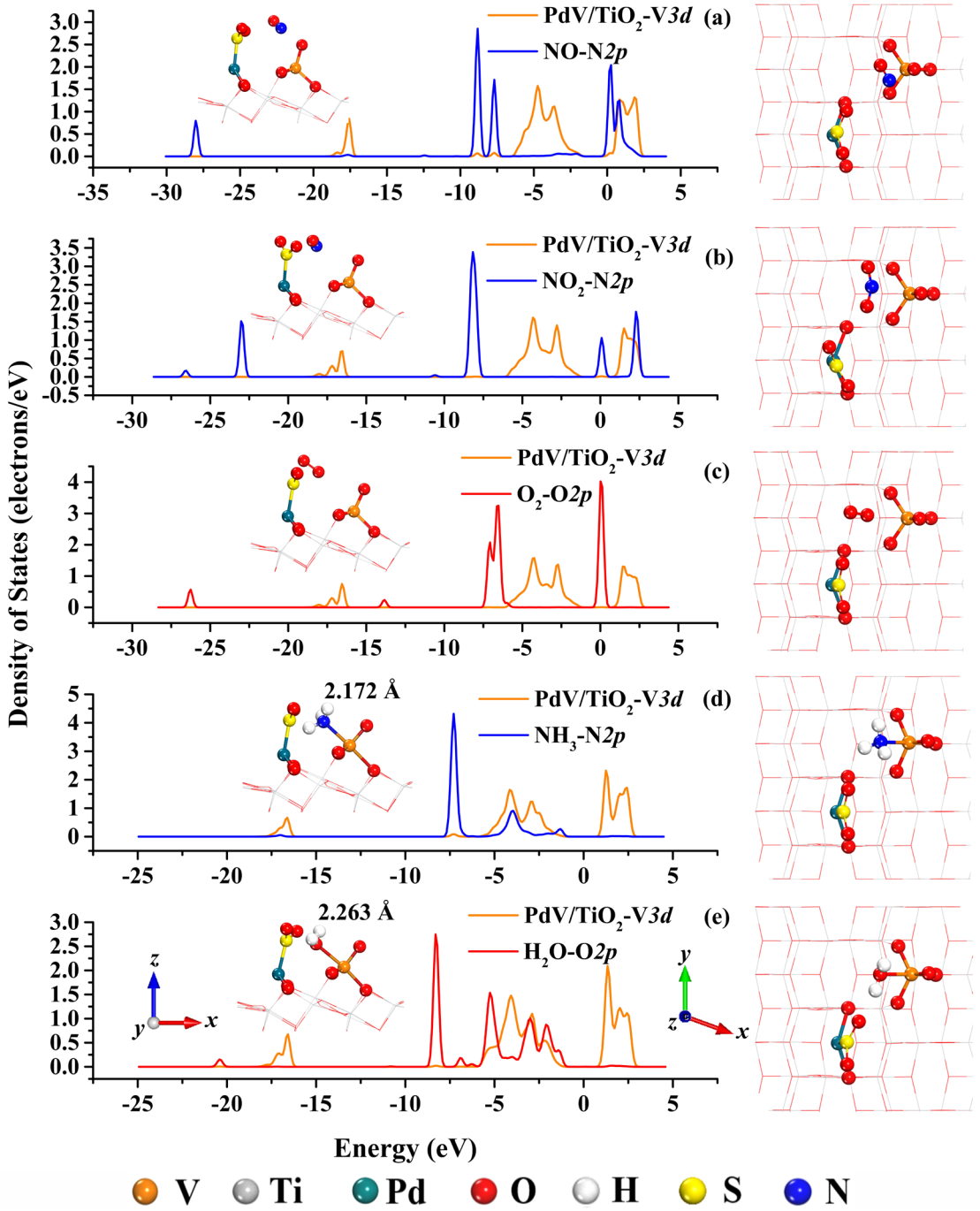

Fig.S11 Co-adsorption configurations and PDOS of SO_2 with NO, NO_2, O_2, NH_3, and H_2O gas molecules on the multi-active center catalyst surface (a-e), respectively.

Tab.S7 Adsorption energy and bond information of SO_2 with NO, NO_2, O_2, NH_3, and H_2O gas molecules on the multi-active center catalyst surface

Parameters	NO_2	NO	O_2	NH_3	H_2O
Gas adsorption end	N (--[a])	N (--[a])	O (--[a])	N (N-V)	O (O-V)
Co-adsorption energy (eV)	--	--	--	-6.990	-6.620
Length of formed bond (Å)	--	--	--	2.172	2.263
Bond length of Cl−Pd (Å)	--	--	--	2.150	2.157

a: Does not adsorb on this active center.

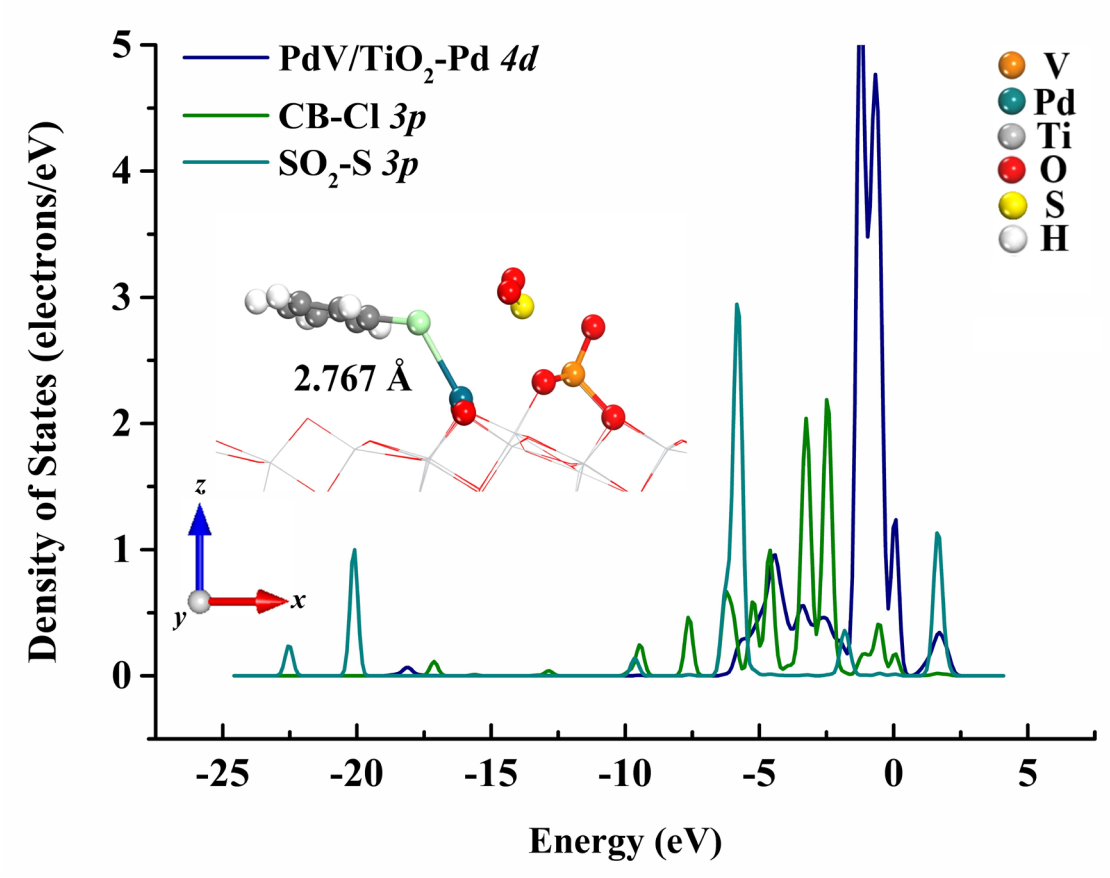

Fig.S12 Competitive adsorption of CB and SO_2 on the multi-active center catalyst surface.

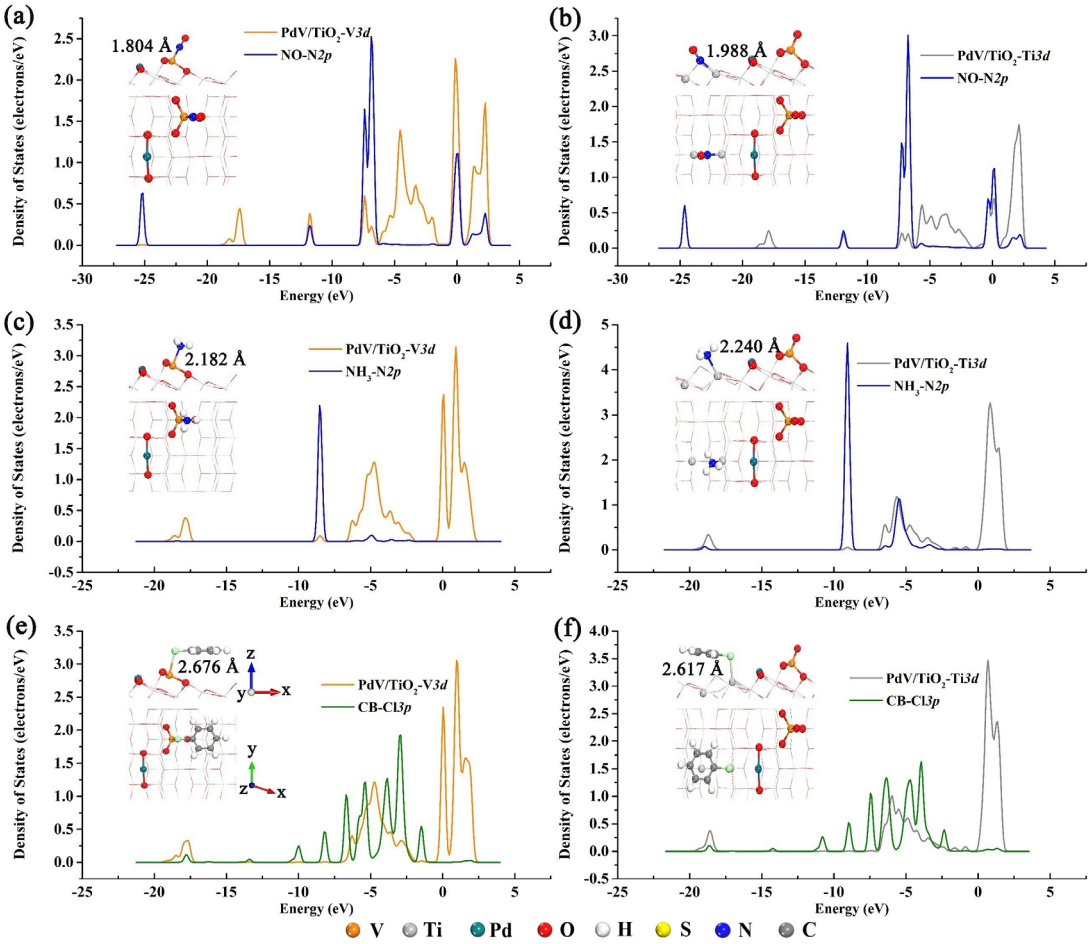

Fig.S13 Adsorption configuration and PDOS of gas molecules (NO, NH_3 and CB) on the generated two O vacancies (a-f), respectively.

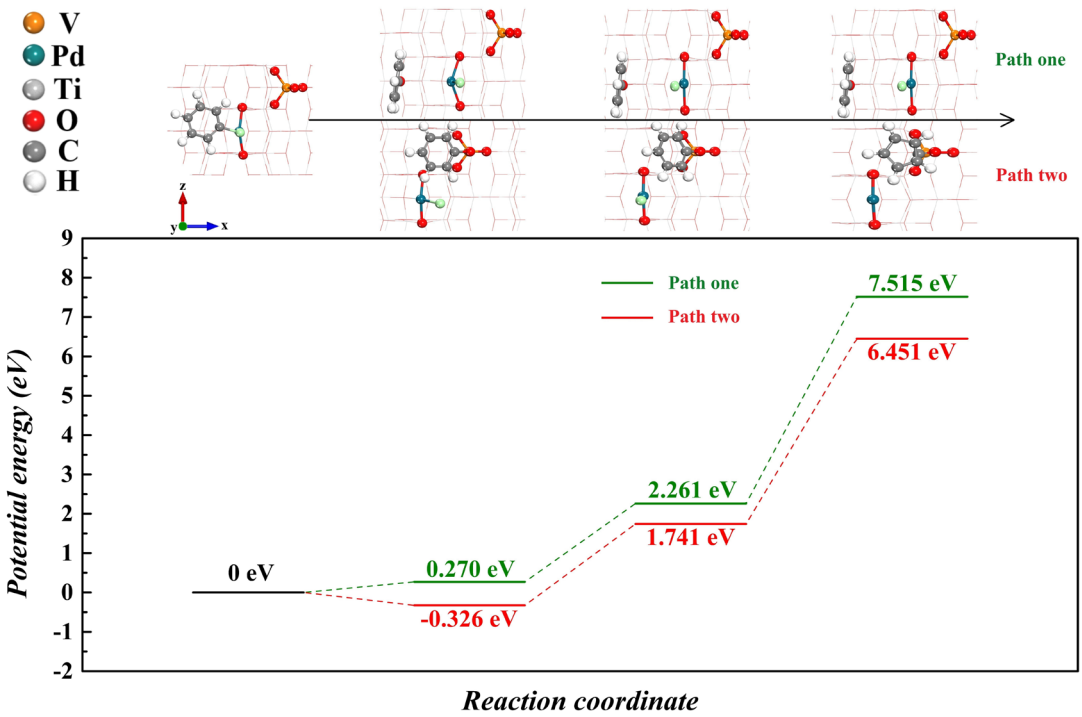

Fig.S14 Removal path and energy barrier of CB on the multi-active center catalyst surface.

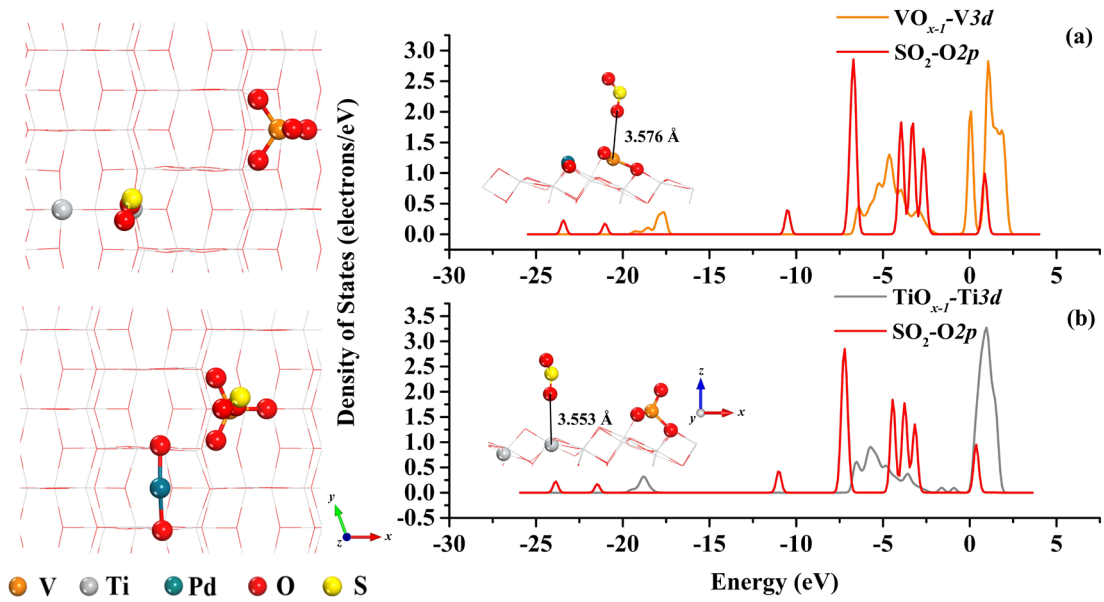

Fig.S15 Configurations and PDOS for SO_2 gas molecule adsorption of the two oxygen vacancies (a and b) on the multi-active center catalyst surface.

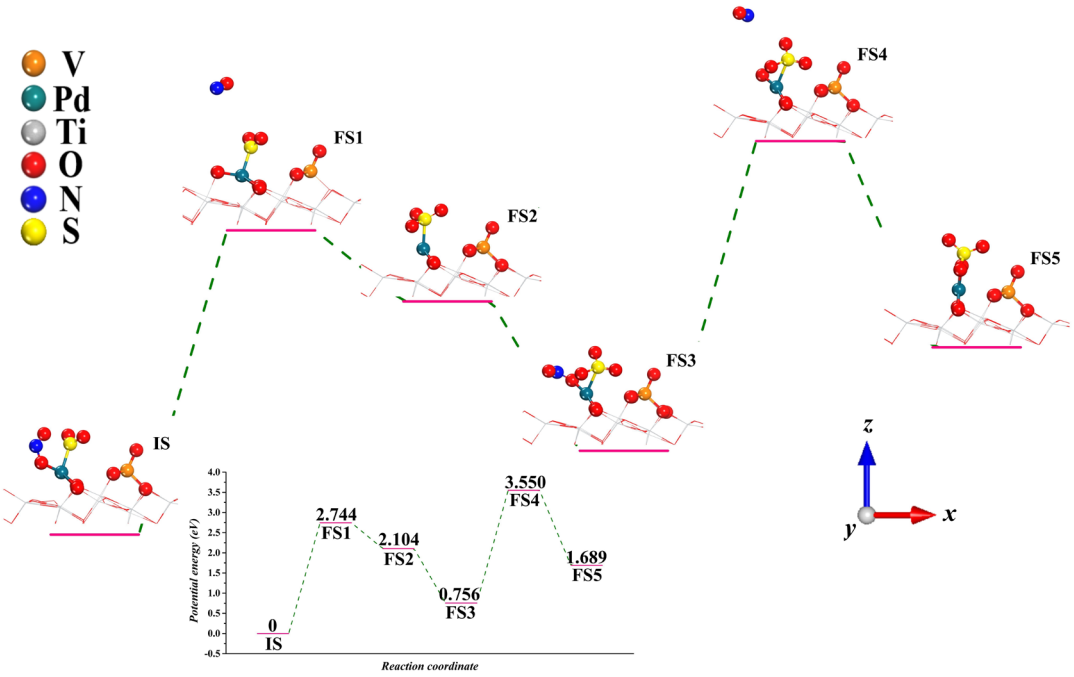

Fig.S16 Oxidation path of $PdSO_4$ by NO_2.

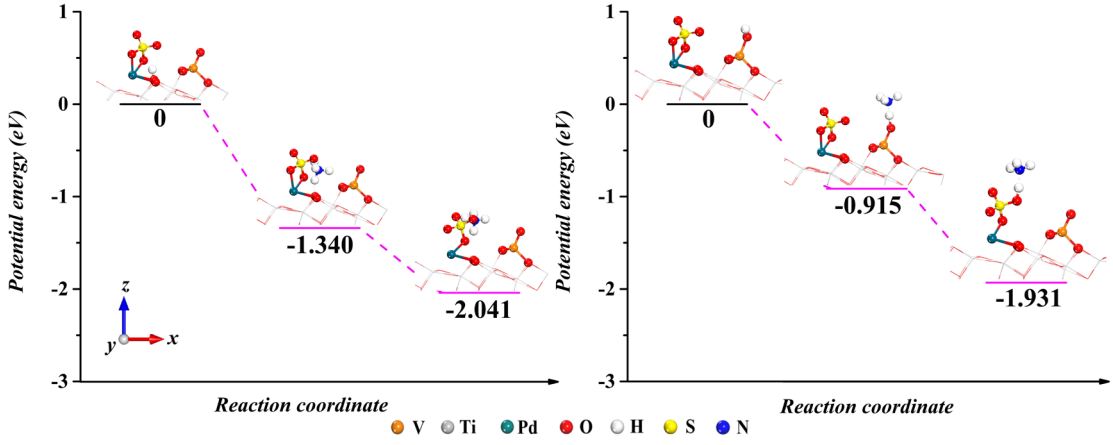

Fig.S17 Generation path of NH_4SO_{4ads} on the multi-active center catalyst surface.

REFERENCES

(1) Brunauer, S.; Emmett, P. H.; Teller, E., Adsorption of gases in multimolecular layers. *J. Am. Chem. Soc.* **1938**, *60*, 309-319.

(2) Lippens, B. C.; Linsen, B. G.; Boer, J. H. D., Studies on pore systems in catalysts I. The adsorption of nitrogen; apparatus and calculation. *J. Catal.* **1964**, *3*, 32-37.

(3) Jain, A.; Hautier, G.; Moore, C. J.; Ong, S. P.; Fischer, C. C.; Mueller, T.; Persson, K. A.; Ceder, G., A High-Throughput infrastructure for density functional theory calculations. *Comp. Mater. Sci.* **2011**, *50*, 2295-2310.

(4) Sun, P. F.; Zhai, S. Y.; Chen, J. K.; Yuan, J. L.; Wu, Z. B.; Weng, X. L., Development of a multi-active center catalyst in mediating the catalytic destruction of chloroaromatic pollutants: A combined experimental and theoretical study. *Appl. Catal. B* **2020**, *272*, 119015-119023.

(5) Jiang, B. Q.; Wu, Z. B.; Liu, Y.; Lee, S. C.; Ho, W. K., DRIFT Study of the SO_2 effect on Low-Temperature SCR reaction over FeMn/TiO_2. *J. Phy. Chem. C* **2010**, *114*, 4961-4965.

(6) Chang, H. Z.; Chen, X. Y.; Li, J. H.; Ma, L.; Wang, C. Z.; Liu, C. X.; Schwank, J. W.; Hao, J. M., Improvement of activity and SO_2 tolerance of Sn-Modified MnO_x-CeO_2 catalysts for NH_3-SCR at low temperatures. *Environ. Sci. Technol.* **2013**, *47*, 5294-5301.

(7) Huang, H.; Gu, Y. F.; Zhao, J.; Wang, X. Y., Catalytic combustion of chlorobenzene over VO_x/CeO_2 catalysts. *J. Catal.* **2015**, *326*, 54-68.

(8) Ma, Z. R.; Wu, X. D.; Si, Z. C.; Weng, D.; Ma, J.; Xu, T. F., Impacts of niobia loading on active sites and surface acidity in NbO_x/CeO_2-ZrO_2 NH_3-SCR catalysts. *Appl. Catal. B* **2015**, *179*, 380-394.

(9) Huang, H.; Gu, Y. F.; Zhao, J.; Wang, X. Y., Catalytic combustion of chlorobenzene over

VO_x/CeO_2 catalysts. *J. Catal.* **2015**, *326*, 54-68.

(10) Amores, J. G.; Escribano, V. S.; Ramis, G.; Busca, G., An FT-IR study of ammonia adsorption and oxidation over Anatase-Supported metal oxides. *Appl. Catal. B* **1997**, *13*, 45-58.

(11) Liu, J.; Li, X. Y.; Li, R. Y.; Zhao, Q. D.; Ke, J.; Xiao, H. N.; Wang, L. D.; Liu, S. M.; Tade, M.; Wang, S. B., Facile synthesis of Tube-Shaped Mn-Ni-Ti solid solution and preferable Langmuir-Hinshelwood mechanism for selective catalytic reduction of NO_x by NH_3. *Appl. Catal. A* **2018**, *549*, 289-301.

(12) Larrubia, M. A.; Busca, G., An FT-IR study of the conversion of 2-chloropropane, o-dichlorobenzene and dibenzofuran on V_2O_5 MoO_3-TiO_2 SCR-DeNO_x catalysts. *Appl. Catal. B* **2002**, *39*, 343-352.

(13) Yan F. P.; Wang Y. H.; Zhang J. Y.; Lin Z.; Sheng, Z. J., Schottky or ohmic Metal-Semiconductor contact: Influence on photocatalytic efficiency of Ag/ZnO and Pt/ZnO model systems. *Chemsuschem* **2014**, *7*, 101-104.

(14) Liu, J. F.; Yu, Y. B.; Mu, Y. J.; He, H., Mechanism of heterogeneous oxidation of carbonyl sulfide on Al_2O_3: An in situ diffuse reflectance infrared fourier transform spectroscopy investigation. *J. Phys. Chem. B* **2006**, *110*, 3225-3230.

(15) Hetrick, C. E.; Lichtenberger, J.; Amiridis, M. D., Catalytic oxidation of chlorophenol over V_2O_5/TiO_2 catalysts. *Appl. Catal. B* **2008**, *77*, 255-263.

(16) Chen, Z. H.; Yang, Q.; Hua, L.; Li, X. H.; Tsang, S. C., Cr-MnO_x Mixed-Oxide catalysts for selective catalytic reduction of NO_x with NH_3 at low temperature. *J. Catal.* **2012**, *276*, 56-65.